Research Article / Review Article FUPRE JOURNAL 7(1): 55-70 (2023)

FUPRE Journal

of

Scientific and Industrial Research

ISSN: 2579-1184(Print) ISSN: 2578-1129 (Online)

http://fupre.edu.ng/journal

TB-mBJ Predictions of Thermoelectric and Optical Properties of Half-Heusler RuVBi alloy

***NENUWE, N. O.*[1,*], *UMUKORO, J.*[2]**

[1]*Address – Institution (University, Department), Postal Code if available, City, Country*

[2]*Address – if second authors exist*

[3]*Address – if third and more authors exist*

ARTICLE INFO

Received: 19/11/2022
Accepted: 24/02/2023

Keywords

Figure of merit, half-Heusler, RuVBi, thermoelectric, structural properties,

ABSTRACT

The thermoelectric and optical properties of the half-Heusler RuVBi compound were predicted using density functional theory (DFT). In other to have a precise band gap, the Tran-Blaha-modified Becke-John (TB-mBJ) approximation is employed. First, the formation energies were determined, and three structural phases were evaluated. The band structure and density of states of the RuVBi compound demonstrated semiconductor behaviour in the α phase and metallic behaviour in the other two phases. The TB-mBJ method was used to analyse the optical properties like dielectric function, reflectivity, conductivity, absorption, refractive index, and electron-energy-loss (eel). Thermoelectric (TE) properties, such as the figure of merit (ZT), Seebeck coefficient (S), electronic conductivity (σ/τ), thermal conductivity (κ/τ), and power factor (PF), were further examined using Boltzmann's transport theory. Based on these findings, RuVBi is a promising candidate for thermoelectric and optoelectronics device applications.

1. INTRODUCTION

The fascinating characteristics and applications of full-Heusler and half-Heusler (hH) compounds have led to great interest in the study of these materials. The chemical formula of hH compounds is represented by XYZ. Here, X and Y denote transition metals, and Z is from the main group elements (Graf et al., 2011; Offernes et al., 2007). Usually, hH compounds have 18 valence electrons in their unit cell, attaining a cubic crystal structure, and several such materials have been studied (Gautier et al., 2015; Kulkova et al., 2006; Osafile & Nenuwe, 2021). Research on hH compounds shows that they behave as semiconductors with a range of energy band gaps and optical properties suitable for solar cell applications and energy storage devices (Casper et al., 2012; Chadov et al., 2010; Kieven et al., 2010; Mehmood & Ahmad, 2018). Half-Heusler compounds also exhibit striking thermoelectric properties that qualify them as thermoelectric materials for power generation over a range of temperatures (Berche et al., 2017; Chen & Ren, 2013; Fu et al., 2012, 2015;

*Corresponding author, e-mail: *nenuwe.nelson@fupre.edu.ng*
DIO

Naydenov et al., 2019; Shen et al., 2001; Yadav & Sanyal, 2015; Yu et al., 2009). Furthermore, several other advantages, such as their low cost, abundance in nature, and ease of synthesis, have made it possible for researchers to develop more effective energy conversion materials (Qiu et al., 2010; Zhang et al., 2012). Over the years, several hH compounds with useful TE properties have been discovered; nevertheless, a search for enhancing their efficiency has been unabated (Fang et al., 2018; Liu et al., 2018; Winiarski & Bilińska, 2019; Yang et al., 2008; Zhu et al., 2015). The thermoelectric efficiency of thermoelectric materials is determined by their figure of merit. *ZT* depends on absolute temperature (T), thermal conductivity, Seebeck coefficient, and electrical conductivity. Thus, it is crucial that these parameters are properly improved to design efficient thermoelectric materials.

In addition, the half-Heusler compounds exhibit different structural, thermodynamic, and mechanical properties. Chibani et al. (Chibani et al., 2018) studied the structural, thermoelectric, electronic, and mechanical behaviour of RuVAs, RuVP, and RuVSb alloys using first-principles calculations. The structural, optical, electronic, mechanical, magnetic, and thermoelectric properties of CrScPb and CrTiPb half-Heusler alloys were studied by Dey et al. using first-principles calculations (Dey et al., 2021).

2. MATERIALS AND METHODS

The thermoelectric, structural, and electronic properties were calculated using the full-potential linearised augmented plane wave (FP-LAPW) method, as implemented in the WIEN2k package (Blaha et al., 2020) in the framework of

In our previous work (Nenuwe and Omagbemı, 2022), we examined structural, thermodynamic, mechanical, and electronic properties of RuVZ (Z = As, Bi, Sb) in the α-phase of half-Heusler compounds. Where the Perdew_Burke Erzherhof (PBE) approximation was employed to analyze the properties of RuVBi within the Quantum Espresso computational code.

In the present work, we considered the optical and thermoelectric properties of RuVBi. Also, we further examined the structural, and electronic properties of RuVBi in three structural phases (α, β, and γ) using the Tran-Blaha-modified Becke-John (TB-mBJ) approximation as executed in WIEN2K code. To the best of our knowledge, the prediction of optical and thermoelectric data for RuVBi half-Heusler alloy is appearing in the literature for the first time.

It was observed that the compound behaves as a non-ferromagnetic semiconductor with an indirect bandgap in the α-phase and exhibits a metallic nature in both the β and γ phases. In addition, a significant thermoelectric efficiency was observed for this new compound.

This paper is organised as follows. First, we report the introduction in Section 1, then describe the computational method used to investigate the optical and thermoelectric properties of RuVBi in Section 2, followed by a discussion of the results obtained in Section 3 and a brief conclusion in Section 4. density functional theory (Hohenberg & Kohn, 1964). The exchange-correlation potential is described by the generalised gradient approximation (GGA) within the scheme of Perdew-Burke_Ernzerhof (PBE) scheme (Perdew et al., 1996). The GGA-PBE approximation is well known underestimates the band gap for strongly

localised d-orbital systems. To overcome these limitations, the Tran-Blaha-modified Becke–Johnson (TB-mBJ) potential (Tran & Blaha, 2009) was employed to study the electronic properties. The total energy was determined using a set of 165 k-points in the irreducible sector of the Brillouin zone, which is equivalent to (17×17×17) Monkhorst-Pack. A value of 8 was used for the plane wave cut-off, and the energy cut-off was set to -6.0 Ry. The Muffin-tin radii (RMT) of RuVBi are respectively taken to be (2.35 for Bi and 2.24 for Ru and V in α-phase), (2.35 for Bi, 2.24 for Ru and 2.18 for V in β-phase), and (2.31 for Bi, 2.25 for Ru and 2.09 for V in γ-phase). The convergence criterion for the total energy was set to 10^{-4} Ry. The thermoelectric parameters were calculated using the Boltzman transport theory as implemented in BoltzTrap code (Madsen et al., 2018). We used a denser grid of (21×21×21) k-ponts for the transport calculation.

3. RESULTS AND DISCUSSION

3.1 Structural and electronic properties

The half-Heusler RuVBi crystallises in the cubic crystal structure $C1_b$, belonging to space group F-43 m (No. 216). The Wyckoff positions for half-Heusler XYZ are 4a(0, 0, 0), 4b(0.5, 0.5, 0.5), and 4c(0.25, 0.25, 0.25). Depending on the atomic positions, three different structural phases can be derived: α-phase (4c, 4b, 4a), β-phase (4b, 4a, 4c), and γ-phase (4a, 4c, 4b). Therefore, in this study, we considered the three structural phases of the RuVBi compound. The ground-state total energies of the α, β, and γ phases of the RuVBi half-Heusler compound were computed and are presented in Table 1. We employed the Murnaghan equation of state (Tyuterev & Vast, 2006) given by Equation (1) for the volume optimisation and structural parameters.

$$E - E_0 = \left[\frac{V_0}{B'} + \frac{V_n}{B'(B'-1)} + \frac{1}{(1-B')}\right] \quad (1)$$

Here, B and B' represent the bulk modulus and its derivative, respectively, E_0 is the ground state energy, and V_0 is the equilibrium volume. With the help of Eq. (1), we plotted the variation in the total energy with respect to the volume for the three phases, as shown in Figure 1(a). This graph can help obtain the minimum energy. It is well known that the phase with the lowest ground-state energy is the most stable. Therefore, we observed that the α-phase of RuVBi is the most stable among the three phases examined in this work. The calculated results for the lattice constants, bulk modulus, and pressure derivative are presented in Table 1. In addition, to confirm the stability and feasibility of the studied hH, the formation energy was computed using equation (2) (Huang et al., 2012; Yakoubi et al., 2012).

$$E_f = \frac{E_T - xE_{Ru} - yE_V - zE_{Bi}}{(x+y+z)} \quad (2)$$

Here, E_T is the total energy of the compound; E_{Ru}, E_V and E_{Bi} represent the total energy of the pure elements Ru, V, and Bi, respectively; and x, y, and z are the numbers of Ru, V, and Bi atoms in the primitive cell, respectively. The calculated total energies, energies of the constituent atoms, and formation energies are listed in Table 1. We observed that the formation energies of the α and γ phases were negative, which signified the feasibility of the compound and established the possible formation of RuVBi under ambient conditions in these phases.

The band structures and density of states provide sufficient information on the electronic properties of solids. We

presented the band structure and projected density of states calculated using the TB-mBJ method which is more accurate. This is because PBE often underestimates energy band gaps due to self-interaction errors (Dey et al., 2021; Heyd et al., 2005), and this has been corrected by applying the TB-mBJ exchange functional (Koller et al., 2012). The band structures of RuVBi in the α-, β-, and γ-phases are shown in Figure 2. In the α-phase of RuVBi (Figure 2a), the obtained band structure shows that the valence band maximum (VBM) lies almost along the Fermi level (E_f) at the L-path, while the conduction band maximum (CBM) lies along the X-path of the Brillouin zone, which indicates that RuVBi is an indirect band gap semiconductor. The band gap obtained through the PBE method was 0.25 eV. However, when employing the TB-mBJ approximation, the band gap value is 0.69 eV. We hoped to obtain experimental values of RuVBi for a better comparison because calculating the band gap with TB-mBJ yields satisfactory results when compared to experiments. For the beta and gamma phases, the band structures obtained from the PBE and TB-mBJ approximations reveal that both the VBM and CBM cross E_f, indicating metallic behaviour with a band gap of (Eg = 0.0 eV), as reported in Table 1.

Table 1: Calculated equilibrium lattice constant $\boldsymbol{a_0}$(Å), bulk modulus B_0(GPa), $\boldsymbol{B_0'}$, band gap E_g(eV), total energy and formation energy E_f(Ry) for RuVBi**.**

Phase	$\boldsymbol{\alpha}$	$\boldsymbol{\beta}$	$\boldsymbol{\gamma}$
$\boldsymbol{E_T}$**(Ry)**	-54125.415	-54125.236	-54125.364
$\boldsymbol{E_{Ru}}$**(Ry)**	-9063.629	-9063.629	-9063.629
$\boldsymbol{E_V}$**(Ry)**	-1898.627	-1898.627	-1898.627
$\boldsymbol{E_{Bi}}$**(Ry)**	-43163.073	-43163.073	-43163.073
$\boldsymbol{E_f}$**(Ry)**	-0.027	0.031	-0.011
$\boldsymbol{a_0}$(Å)	6.18	6.25	6.17
$\boldsymbol{B_0}$**(GPa)**	143.428	122.326	130.952
$\boldsymbol{B_0'}$	4.99	4.67	4.56
$\boldsymbol{E_g}$**(eV)**	0.25^{PBE}	0.00^{PBE}	0.00^{PBE}
	0.69^{mBJ}	0.00^{mBJ}	0.00^{mBJ}

In addition, we plotted the projected density of states for the α-phase of RuVBi, as shown in Figure 2(d). We observed that contributions to the band gap in the conduction and valence bands are mainly from the d-orbital and doubly degenerate states (d-eg) of the transition metals Ru and V. The VBM and CBM of the RuVBi compound were formed by Ru (d-eg) and V(d-orbital) interactions. This is responsible for the hybridisation gap.

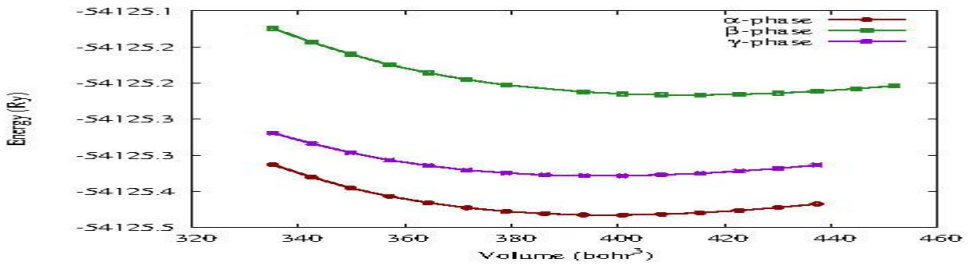

Figure 1. Calculated total energy versus volume for RuVBi half-Heusler.

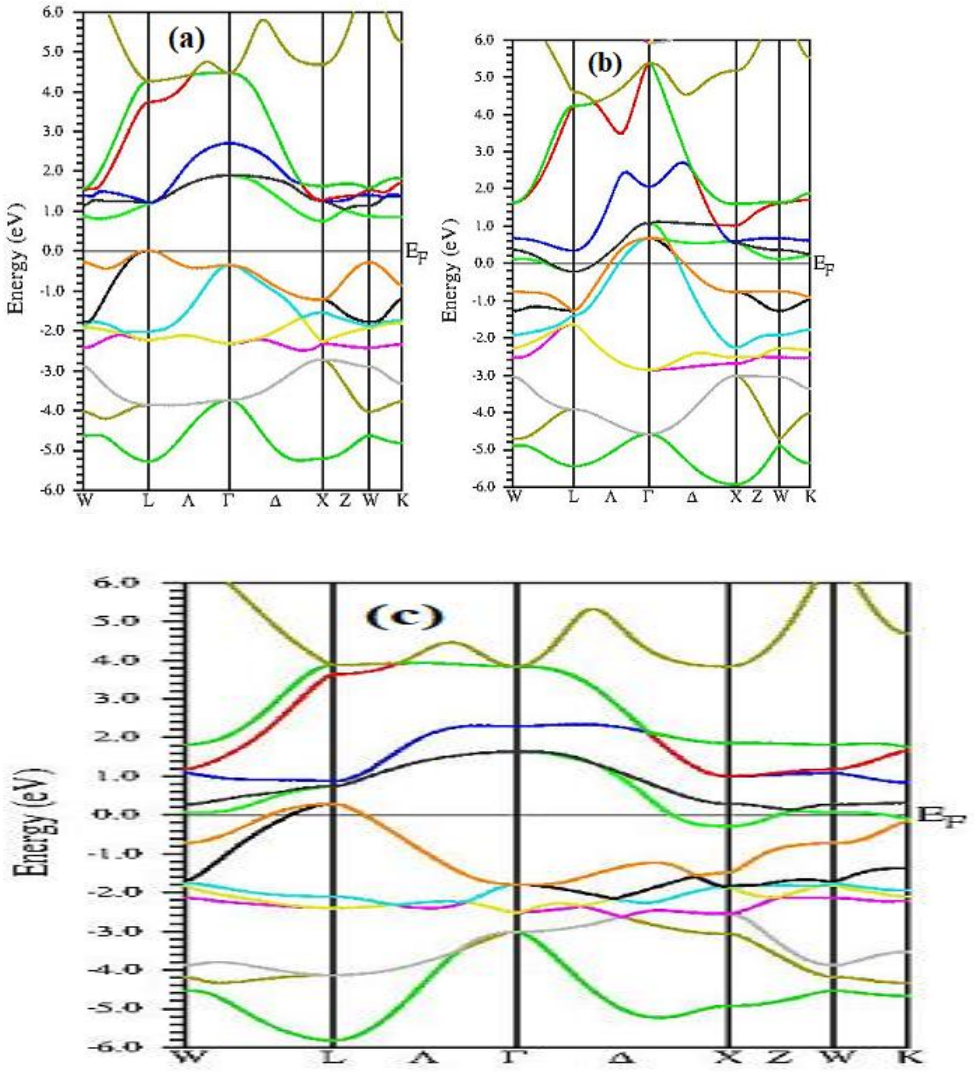

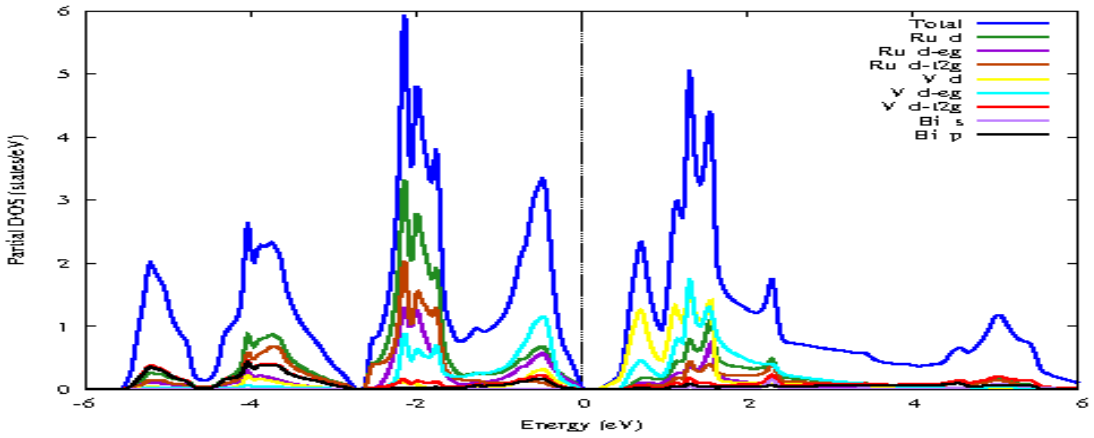

Figure 2. Calculated band structure for (a) α-RuVBi, (b) β-RuVBi, (c) γ-RuVBi, and (d) density of states for α-RuVBi

3.2 Thermoelectric properties of RuVBi

Herein, we present the temperature-dependent TE properties of the RuVBi half-Heusler material. The parameters considered are the figure of merit, Seebeck coefficient, electrical conductivity divided by relaxation time, thermal conductivity divided by relaxation time, and power factor. These parameters were calculated from the semi-classical transport equation as implemented in the BoltzTrap computational code (Madsen & Singh, 2006). Using the rigid band approach, S, σ, and κ were calculated using the following relations:

$$\sigma = e^2 \int \Xi_{i,k} \left(-\frac{\partial f_0(\varepsilon,T,\mu)}{\partial \varepsilon}\right) d\varepsilon \quad (3)$$

$$\kappa = k_B^2 T \int \Xi_{i,k} \left(\frac{\varepsilon-\mu}{k_B T}\right)^2 \left(-\frac{\partial f_0(\varepsilon,T,\mu)}{\partial \varepsilon}\right) d\varepsilon \quad (4)$$

$$S = \frac{e k_B}{\sigma} \int \Xi_{i,k} \left(\frac{\varepsilon-\mu}{k_B T}\right) \left(-\frac{\partial f_0(\varepsilon,T,\mu)}{\partial \varepsilon}\right) d\varepsilon \quad (5)$$

Where the transport distribution function is given as

$$\Xi_{i,k} = \sum_{ik} v_m v_n \tau_k \quad (6)$$

where, m, n are tensor indices, v_m and v_n represent the group velocities, e is the electron charge, τ_k is the relaxation time, k_B is the Boltzmann constant and f_0, denotes the Fermi-Dirac distribution. The electron contribution is in the range of the chemical potential: $\mu - k_B T < \varepsilon < \mu + k_B T$. The dimensionless figure-of-merit is calculated using the following relation:

$$ZT = \frac{S^2 \sigma T}{\kappa} \quad (7)$$

From Eq. (7), ZT is directly proportional to S and inversely proportional to κ. Therefore, high values of the figure of merit can be derived from small values of the thermal conductivity and a large Seebeck coefficient. The TE efficiency ZT~1 is considered the threshold for practical applications of thermoelectric materials (Heremans et al., 2008). The power factor is another significant parameter to be considered when examining the transport capabilities of TE materials. It is defined as $\mathrm{PF} = (S^2\sigma)/\tau$.

The thermoelectric parameters were investigated at temperatures ranging from 300 to 1200 K. Figure 3 shows how the TE parameters depend on temperature. One of the most essential metrics of TE materials is the Seebeck coefficient, which is often known as thermopower. The *S* measures the magnitude of the thermoelectric voltage generated by the Seebeck effect when the temperature of a material varies. Figure 3(a) shows that the value of Seebeck coefficient increases with increasing temperature. The *S* value of RuVBi is about 83.82 μV/K at 300 K but increased significantly to about 172.17 μV/K at 1100 K. The positive value of *S* in the entire temperature range is an indication that holes are the dominant carriers, and therefore, RuVBi is a p-type material. This trend is similarto the findings of Rai et al. (Rai et al., 2016) for ZrxHr1-x-yTay thermoelectric materials. Figure 3(b) depicts the electronic conductivity per relaxation time(σ/τ), which describes the electronic conductance of the material because of electron movement from high-to low-temperature regions. The electronic conductivity data increased as the temperature increased, indicating that the material is a semiconductor. Because resistivity is essentially the inverse of conductivity, the results are equivalent to the resistivity curve, suggesting that resistivity of semiconductor decreases as temperature increases. Thermal conductivity is made up of contributions from both the electron and lattice conductivities. The BoltzTrap code computes only the electronic contribution. Low thermal conductivity is required to improve the performance of TE devices. The electronic thermal conductivity per relaxation time (κ/τ) versus temperature plot is shown in Figure 3(c). As the temperature increases, the thermal conductivity increases to a maximum of 1.84 x 10^{15} W/msK. Figure 3(d) shows the power factor-temperature relationship. *PF* is a crucial parameter in determining the transport characteristics of thermoelectric materials. It increases in direct proportion to temperature. Typically, RuVBi has a value of 28.57 x 10^{10} W/msK^2 at 300 K. It reaches a maximum value of of 222.9 x 10^{10} W/msK^2 at 1200 K. In addition, as shown in Figure 3(e), we determined the dimensionless figure of merit, which is the most important metric that characterizes the efficiency of thermoelectric materials. *ZT* ranges from 0.32 at ambient temperature to 1.46 at 1100 K, according to the curve. Our room temperature value is greater than Synoradzki et al. experimental findings for the half-Heusler ScNiSb (Synoradzki et al., 2019). The peak value of 1.46 is notable because it exceeds the ZT~1 threshold, suggesting that the alpha-type RuVBi half-Heusler material is a promising contender for thermoelectric applications.

The predicted TE properties for RuVBi at room temperature are displayed in Figure 4 (a – c). When the Fermi level is at the centre of the band gap, the Seebeck coefficient is significant, and it rapidly declines to zero when the Fermi level exits the band gap and penetrates deeply into the valence and conduction bands, as shown in Figure 4(a). The *PF* has low values when the Fermi level is near the bandgap, as shown in Figure 4(b). This is because of the low carrier concentration and, as a result, the low electronic conductivity. The hole or electron concentration increases exponentially when the Fermi level shifts down the valence band or upward into the conduction band, resulting in an increase in the electronic conductivity and power factor (Figure 4c). *PF* attains its highest value near the band edge at a specific Fermi level. This trend was observed by

Yang et al. (Yang et al., 2008), who investigated the electronic transport properties of TiCoSb, ZrNiSn, and LaPbBi half-Heuslers.

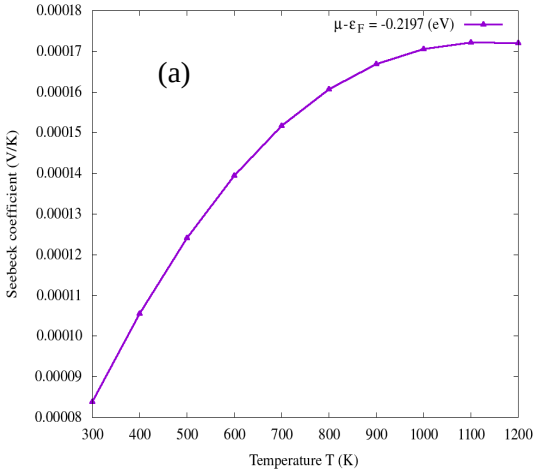

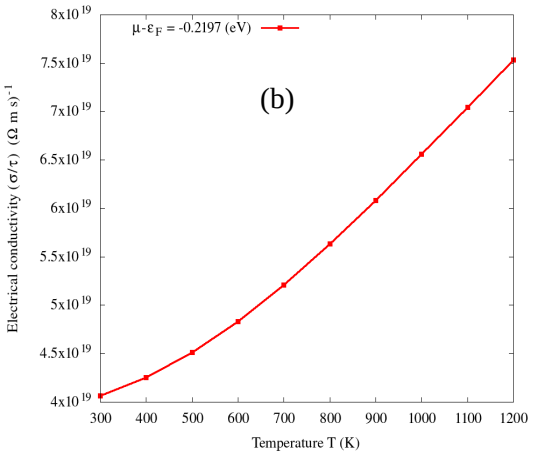

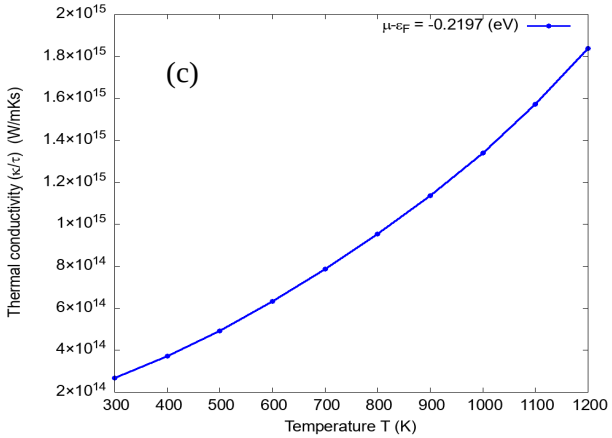

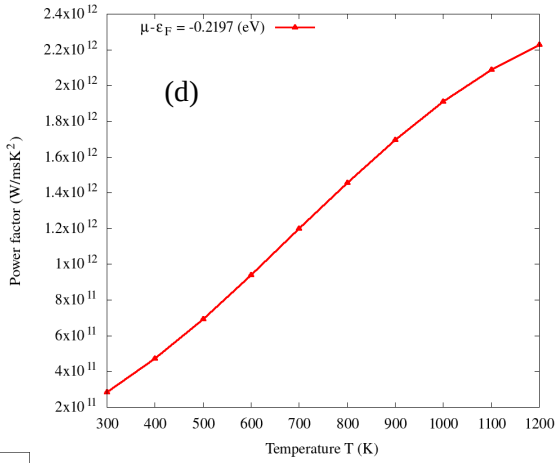

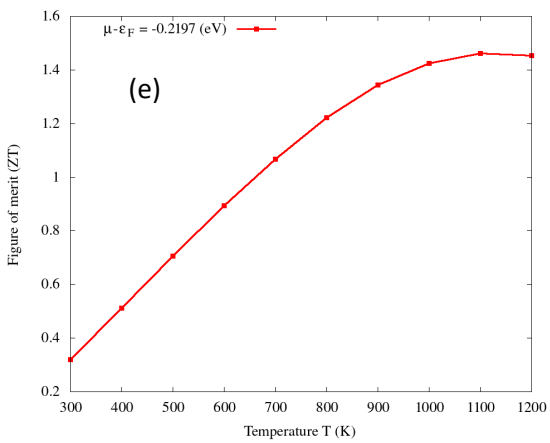

Figure 3. Calculated temperature dependent (a) Seebeck coefficient *S*(V/K), (b) Electrical conductivity $\frac{\sigma}{\tau}(\boldsymbol{\Omega ms})^{-1}$, (c) Thermal conductivity $\frac{\kappa}{\tau}$ $(\boldsymbol{W/mKs})$, (d) Power factor (W/msK^2) and (e) *ZT* of RuVBi.

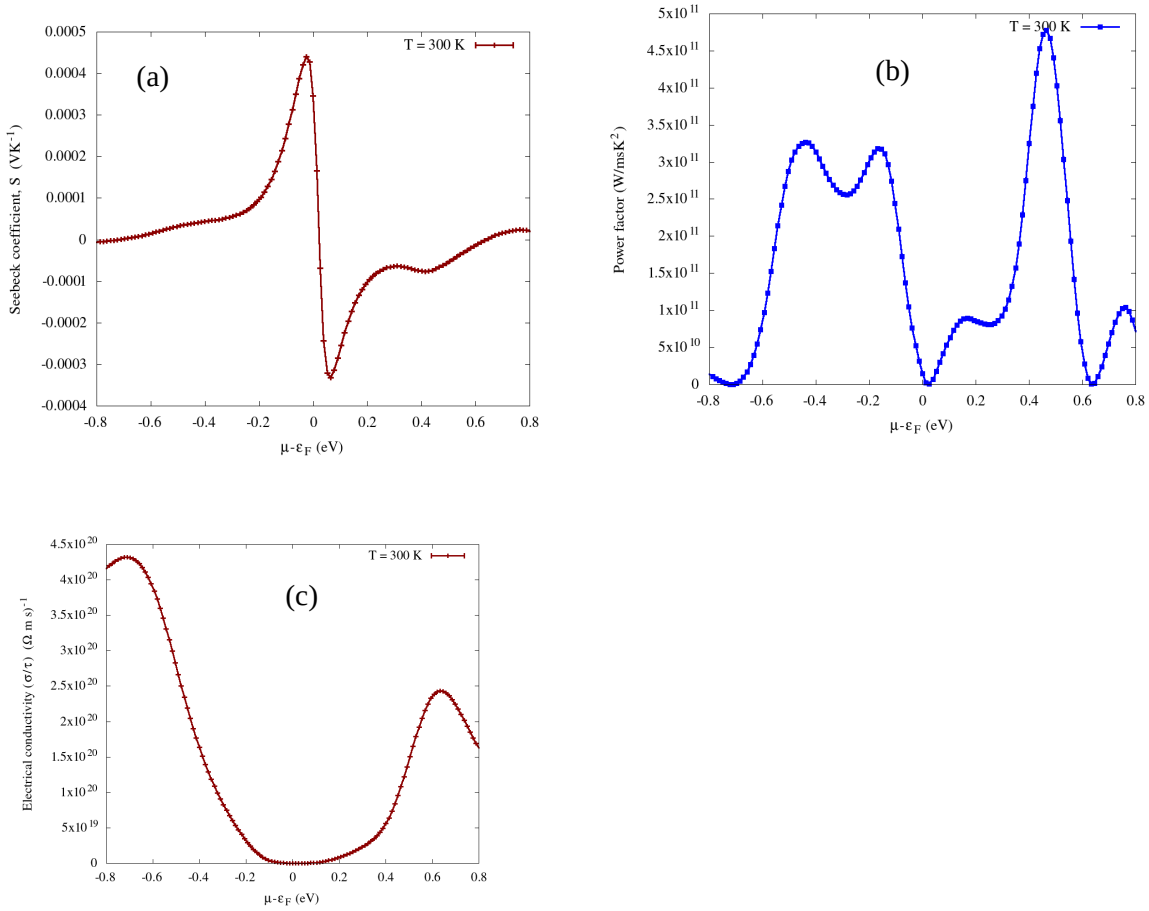

Figure 4. Calculated chemical potential (μ-ε$_f$) dependent (a) Seebeck coefficient *S*(V/K), (b) Power factor (W/msK^2) and (c) Electrical conductivity σ/τ (Ωms)$^{-1}$ of RuVBi.

3.3 Optical properties of RuVBi

Optical properties play an important role in the optoelectronic properties of materials.

The optical properties of RuVBi are examined by the complex-dielectric equation: $\varepsilon(\omega) = \varepsilon_1(\omega) + \varepsilon_2(\omega)$. Where $\varepsilon_1(\omega)$ and $\varepsilon_2(\omega)$ are the real and imaginary parts of the dielectric function. The $\varepsilon_2(\omega)$ is calculated in WIEN2K numerically by using the independent-particle approximations and Kohn-Sham eigen values to evaluate the direct transitions between the occupied and unoccupied states. The Krammers-Kronig transition of the resulting imaginary part of the dielectric function $\varepsilon_2(\omega)$ gives the real part $\varepsilon_1(\omega)$. And the other optical parameters such as reflectivity, conductivity, absorption, refractive index, and electron-energy-loss (eel) are calculated from $\varepsilon_2(\omega)$. The calculated results for the optical properties are shown in Figure 5 for the energy range up to 13.56. To the best of our knowledge there is no theoretical and experimental optical properties available for RuVBi half-Heusler in literature.

Figure 5(a) reports the real and imaginary (ε_1 and ε_2) components of the dielectric function of the RuVBi half-Heusler. Under an incident light-energy, $\varepsilon_1(0)$ denotes the electronic polarizability (Djelti et al., 2020). At zero frequency, the static dielectric is equal to 27.31. The reduction in $\varepsilon_1(0)$ and the appearance of negative values after it reached its highest value of 44.32 (at 1.18 eV) is because the RuVBi alloy completely reflects the incident radiation. In the energy range of 3.143 to 13.565 eV, $\varepsilon_1(\omega)$, displays negative values. RuVBi material is extremely useful in energy recovery devices due to its strong absorption at low incident energy. The imaginary part of the dielectric $\varepsilon_2(\omega)$, which is associated with the absorption of the incident energy due to the various electronic transitions generated by the impart energies larger than the band gap, describes the light-absorption by RuVBi half-Heusler. The $\varepsilon_2(\omega)$ may have been influenced by the intra-band and inter-band transitions. . In the low energy area (visible), where there is little light dispersion, $\varepsilon_2(\omega)$ starts at 0 eV and reaches a maximum value of 32 (at 1.89 eV). The transition between the lowest unoccupied conduction band of V-3d states and the highest occupied valence band of Ru-3d states is what led to formation of this peak value.

Figure 5(b) represents the real part of refractive index of RuVBi alloy. The static refractive index n(0) of RuVBi is found to be 5.22 and increases to its peak value of 6.75 around photon energy of 1.18 eV near the the ifrared-region. The static refractive index obtained in this study is comparable to the results obtained from previous studies of Heuslers and half-Heuslers compounds. The refractive index of Fe2ScAs and Fe2ScP (Ali & Rahaman, 2018) LiScSi (Ciftci & Evecen, 2018) and AgScSi (Kars Durukan & Öztekin Çiftci, 2019) alloys is 7.2, 6, 4.6, and 4.51, respectively. In the range of energy considered in this work, the refractive index value remain positive suggesting linearity of RuVBi to the frequency of light (Yaqoob et al., 2019).

Figure 5(c) shows the optical reflectivity of RuVBi as a function of incident photon energy. The optical reflectivity determines behavior of surface of the studied material. We observed that the reflectivity of RuVBi begins with a value of approximately 0.46 rising and then falling and then rising again to reach a maximum value of ~0.75 between 0.013 eV and 13.56 eV.

The electron energy loss (eel) function of compounds is a key optical parameter to explain the energy loss of a fast electron passing through a sloid which is usually large at plasma frequency (Xu et al., 2006). Figure 5(d) represents the eel function of RuVBi half-Heusler. We noticed three prominent peaks at 0.159 eV,

0.211 eV, and 0.522 eV, which suggests rapid increase in the reflectance. These peaks are connected to plasma resonance and the corresponding frequency is usually called plasma frequency (Ali & Rahaman, 2018; Rahman et al., 2016). The conductivity spectrum of RuVBi alloy is shown in Figure 5(e). The observed optical photo conductivity has several maximum and minimum within the energy range examined. Since RuVBi has small band gap as shown in the band-structure calculations, the photo conductivity starts from ~0.0136 eV as shown in Figure 5(e).

The absorption coefficient predicts how long photon frequency can enter a material before being completely absorbed (Ali et al., 2016). The absorption spectra of RuVBi as shown in Figure 5(f) reveal the semiconducting nature of RuVBi, since the spectra begin from 0.0136 eV. Three peaks have been observed at 3.74 eV, 6.41 eV and 9.48 eV. This material possesses good absorption coefficient near the ultraviolet region.

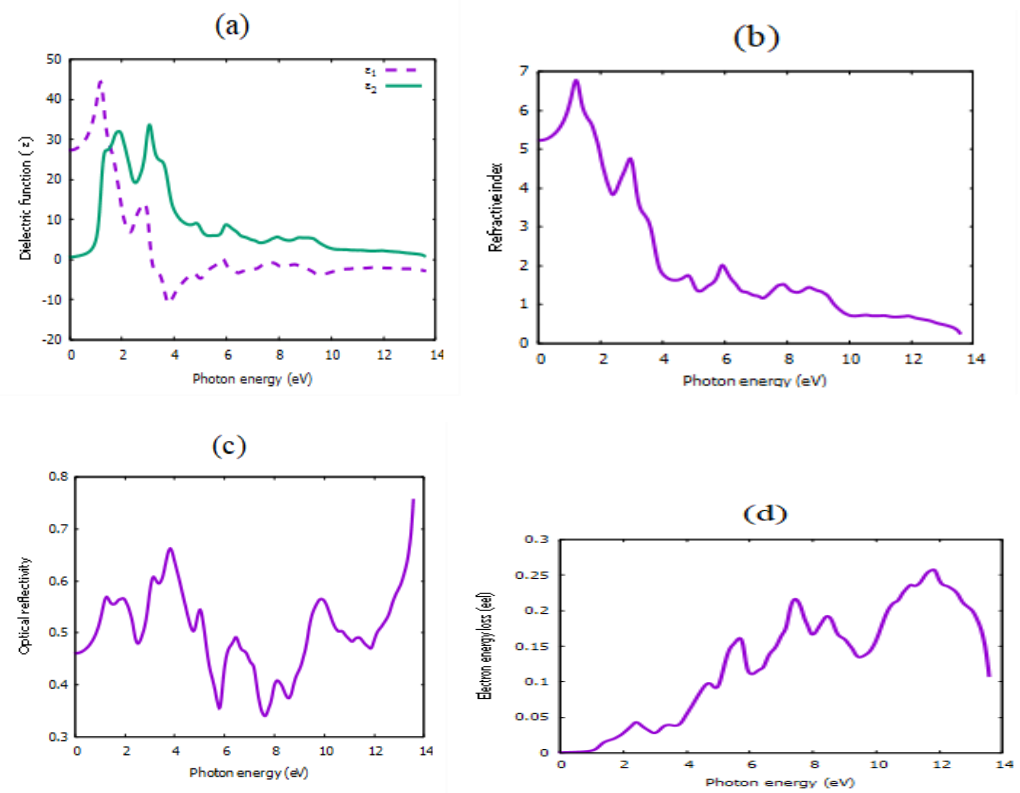

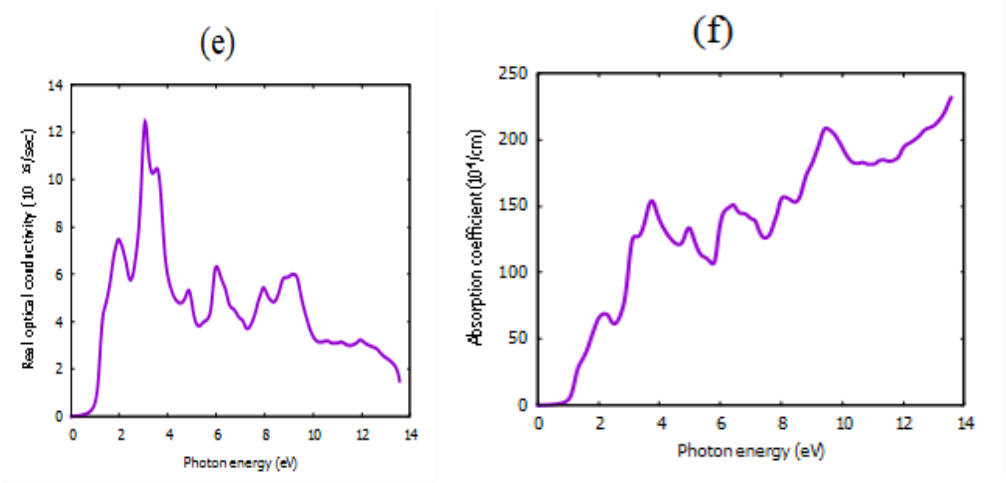

Figure 5. (a) Dielectric function, (b) refractive index (c) optical refletivity (d) electron energy loss (e) real optical conductivity (f) absorption coefficient for RuVBi half-Heusler by employing TB-mBJ approximation.

4. CONCLUSIONS

The thermoelectric, and optical properties of the half-Heusler RuVBi compound were investigated using the FP-LAPW technique. The results revealed that the RuVBi half-Heusler is most stable in the α-phase with a non-ferromagnetic structure. By investigating the electronic properties with TB-mBJ, we discovered that RuVBi is a semiconductor in the alpha phase and metallic in both beta and gamma phases. In addition, we used the BoltzTrap package to examine the thermoelectric properties. Research on thermoelectric characteristics demonstrates that the examined material exhibits significant thermoelectric behaviour even at high temperatures. Thus, the RuVBi half-Heusler compound can be used in thermoelectric device applications. Futhermore, the optical properties of RuVBi are found to vary according to phonon energies and may be considered suitable for photoelectronic applications.
Furthermore, we discovered that the optical properties of RuVBi fluctuate with phonon energies and this compound might be suitable for photoelectronic applications.

Acknowledgements

The authors acknowledge Prof. Ben Iyozor of the University of Benin for productive discussions during this study.

References

Ali, M. L., & Rahaman, M. Z. (2018). Investigation of different physical aspects such as structural, mechanical, optical properties and Debye temperature of Fe2ScM (M=P and As) semiconductors: A DFT-based first principles study. *International Journal of Modern Physics B*, *32*(10). https://doi.org/10.1142/S0217979218501217

Ali, M. L., Rahaman, M. Z., & Rahman, M. A. (2016). The structural, elastic and optical properties of ScM (M = Rh, Cu, Ag, Hg) intermetallic compounds under pressure by ab initio simulations. *International Journal of Computational Materials Science and Engineering*, *5*(4).

https://doi.org/10.1142/S2047684116500 24X

Berche, A., Tédenac, J. C., & Jund, P. (2017). Phase separation in the half-Heusler thermoelectric materials (Hf,Ti,Zr)NiSn. *Scripta Materialia*, *139*. https://doi.org/10.1016/j.scriptamat.2017. 06.036

Blaha, P., Schwarz, K., Tran, F., Laskowski, R., Madsen, G. K. H., & Marks, L. D. (2020). WIEN2k: An APW+lo program for calculating the properties of solids. *Journal of Chemical Physics*, *152*(7). https://doi.org/10.1063/1.5143061

Casper, F., Graf, T., Chadov, S., Balke, B., & Felser, C. (2012). Half-Heusler compounds: Novel materials for energy and spintronic applications. In *Semiconductor Science and Technology* (Vol. 27, Issue 6). https://doi.org/10.1088/0268-1242/27/6/063001

Chadov, S., Qi, X., Kübler, J., Fecher, G. H., Felser, C., & Zhang, S. C. (2010). Tunable multifunctional topological insulators in ternary Heusler compounds. *Nature Materials*, *9*(7). https://doi.org/10.1038/nmat2770

Chen, S., & Ren, Z. (2013). Recent progress of half-Heusler for moderate temperature thermoelectric applications. *Materials Today*, *16*(10), 387–395. https://doi.org/10.1016/J.MATTOD.2013 .09.015

Chibani, S., Arbouche, O., Zemouli, M., Benallou, Y., Amara, K., Chami, N., Ameri, M., & el Keurti, M. (2018). First-principles investigation of structural, mechanical, electronic, and thermoelectric properties of Half-Heusler compounds RuVX (X=As, P, and Sb). In *Computational Condensed Matter* (Vol. 16). https://doi.org/10.1016/j.cocom.2018.e00 312

Ciftci, Y. O., & Evecen, M. (2018). First principle study of structural, electronic, mechanical, dynamic and optical properties of half-Heusler compound LiScSi under pressure. *Phase Transitions*, *91*(12). https://doi.org/10.1080/01411594.2018.1 515433

Dey, A., Sharma, R., Dar, S. A., & Raza, H. H. (2021). A Computational Investigation on Structural, Mechanical, Electronic, Magnetic, Thermoelectric, and Optical Properties of CrXPb (X = Sc, Ti) Half-Heusler Alloys. *Journal of Superconductivity and Novel Magnetism*, *34*(3). https://doi.org/10.1007/s10948-020-05791-w

Fang, T., Zhao, X., & Zhu, T. (2018). Band structures and transport properties of high-performance half-heusler thermoelectric materials by first principles. In *Materials* (Vol. 11, Issue 5). https://doi.org/10.3390/ma11050847

Fu, C., Bai, S., Liu, Y., Tang, Y., Chen, L., Zhao, X., & Zhu, T. (2015). *ARTICLE Realizing high figure of merit in heavy-band p-type half-Heusler thermoelectric materials*. https://doi.org/10.1038/ncomms9144

Fu, C., Xie, H., Zhu, T. J., Xie, J., & Zhao, X. B. (2012). Enhanced phonon scattering by mass and strain field fluctuations in Nb substituted FeVSb half-Heusler thermoelectric materials. *Journal of Applied Physics*, *112*(12). https://doi.org/10.1063/1.4772605

Gautier, R., Zhang, X., Hu, L., Yu, L., Lin, Y., Sunde, T. O. L., Chon, D., Poeppelmeier, K. R., & Zunger, A. (2015). Prediction and accelerated laboratory discovery of previously unknown 18-electron ABX compounds. *Nature Chemistry*, *7*(4). https://doi.org/10.1038/nchem.2207

Graf, T., Felser, C., & Parkin, S. S. P. (2011). Simple rules for the understanding of Heusler compounds. In *Progress in Solid State Chemistry* (Vol. 39, Issue 1). https://doi.org/10.1016/j.progsolidstchem .2011.02.001

Heremans, J. P., Jovovic, V., Toberer, E. S., Saramat, A., Kurosaki, K., Charoenphakdee, A., Yamanaka, S., & Snyder, G. J. (2008). Enhancement of thermoelectric efficiency in PbTe by distortion of the electronic density of states. *Science*, *321*(5888). https://doi.org/10.1126/science.1159725

Heyd, J., Peralta, J. E., Scuseria, G. E., & Martin, R. L. (2005). Energy band gaps and lattice parameters evaluated with the Heyd-Scuseria-Ernzerhof screened hybrid functional. *Journal of Chemical Physics*, *123*(17). https://doi.org/10.1063/1.2085170

Hohenberg, P., & Kohn, W. (1964). Inhomogeneous electron gas. *Physical Review*, *136*(3B). https://doi.org/10.1103/PhysRev.136.B864

Huang, Z. W., Zhao, Y. H., Hou, H., & Han, P. D. (2012). Electronic structural, elastic properties and thermodynamics of Mg 17Al 12, Mg 2Si and Al 2Y phases from first-principles calculations. *Physica B: Condensed Matter*, *407*(7). https://doi.org/10.1016/j.physb.2011.12.132

Kars Durukan, I., & Öztekin Çiftci, Y. (2019). The Effect of Pressure on Elastic Anisotropy, Vibration and Optical Properties of a AgScSi Compound. *Journal of Electronic Materials*, *48*(6). https://doi.org/10.1007/s11664-019-07167-w

Kieven, D., Klenk, R., Naghavi, S., Felser, C., & Gruhn, T. (2010). I-II-V half-Heusler compounds for optoelectronics: Ab initio calculations. *Physical Review B - Condensed Matter and Materials Physics*, *81*(7). https://doi.org/10.1103/PhysRevB.81.075208

Koller, D., Tran, F., & Blaha, P. (2012). Improving the modified Becke-Johnson exchange potential. *Physical Review B - Condensed Matter and Materials Physics*, *85*(15). https://doi.org/10.1103/PhysRevB.85.155109

Kulkova, S. E., Eremeev, S. v., Kakeshita, T., Kulkov, S. S., & Rudenski, G. E. (2006). The electronic structure and magnetic properties of full- And half-heusler alloys. *Materials Transactions*, *47*(3). https://doi.org/10.2320/matertrans.47.599

Liu, Y., Fu, C., Xia, K., Yu, J., Zhao, X., Pan, H., Felser, C., & Zhu, T. (2018). Lanthanide Contraction as a Design Factor for High-Performance Half-Heusler Thermoelectric Materials. *Advanced Materials*, *30*(32). https://doi.org/10.1002/adma.201800881

Madsen, G. K. H., Carrete, J., & Verstraete, M. J. (2018). BoltzTraP2, a program for interpolating band structures and calculating semi-classical transport coefficients. *Computer Physics Communications*, *231*. https://doi.org/10.1016/j.cpc.2018.05.010

Madsen, G. K. H., & Singh, D. J. (2006). BoltzTraP. A code for calculating band-structure dependent quantities. *Computer Physics Communications*, *175*(1). https://doi.org/10.1016/j.cpc.2006.03.007

Mehmood, N., & Ahmad, R. (2018). Structural, Electronic, Magnetic, and Optical Properties of Half-Heusler Alloys RuMnZ (Z = P, As): a First-Principle Study. *Journal of Superconductivity and Novel Magnetism*, *31*(1). https://doi.org/10.1007/s10948-017-4196-0

Naydenov, G. A., Hasnip, P. J., Lazarov, V. K., & Probert, M. I. J. (2019). Huge power factor in p-type half-Heusler alloys NbFeSb and TaFeSb. *JPhys Materials*, *2*(3). https://doi.org/10.1088/2515-7639/ab16fb

Nenuwe, N. O., & Omagbemı, O. (2022). DFT based Investigation of Structural, Thermodynamic, Mechanical and Electronic Properties of RuVZ (Z: As,

Bi, Sb) Half-Heusler Semiconductors. *VNU Journal of Science: Mathematics - Physics*, *38*(3), 24–37. https://doi.org/10.25073/2588-1124/vnumap.4705

Offernes, L., Ravindran, P., & Kjekshus, A. (2007). Electronic structure and chemical bonding in half-Heusler phases. *Journal of Alloys and Compounds*, *439*(1–2). https://doi.org/10.1016/j.jallcom.2006.08.316

Osafile, O. E., & Nenuwe, O. N. (2021). Lattice dynamics and thermodynamic responses of XNbSn half-heusler semiconductors: A first-principles approach. *Journal of the Nigerian Society of Physical Sciences*, *3*(2). https://doi.org/10.46481/jnsps.2021.174

Perdew, J. P., Burke, K., & Ernzerhof, M. (1996). Generalized gradient approximation made simple. *Physical Review Letters*, *77*(18). https://doi.org/10.1103/PhysRevLett.77.3865

Qiu, P., Yang, J., Huang, X., Chen, X., & Chen, L. (2010). Effect of antisite defects on band structure and thermoelectric performance of ZrNiSn half-Heusler alloys. *Applied Physics Letters*, *96*(15). https://doi.org/10.1063/1.3396981

Rahman, M. A., Rahaman, M. Z., & Rahman, M. A. (2016). The structural, elastic, electronic and optical properties of MgCu under pressure: A first-principles study. *International Journal of Modern Physics B*, *30*(27). https://doi.org/10.1142/S021797921650199X

Rai, D. P., Shankar, A., Sandeep, S., Ghimire, M. P., Khenata, R., & Thapa, R. K. (2016). Correction: Study of the enhanced electronic and thermoelectric (TE) properties of Zr x Hf 1−x−y Ta y NiSn: a first principles study . *RSC Advances*, *6*(16). https://doi.org/10.1039/c6ra90008a

Shen, Q., Chen, L., Goto, T., Hirai, T., Yang, J., Meisner, G. P., & Uher, C. (2001). Effects of partial substitution of Ni by Pd on the thermoelectric properties of ZrNiSn-based half-Heusler compounds. *Applied Physics Letters*, *79*(25). https://doi.org/10.1063/1.1425459

Synoradzki, K., Ciesielski, K., Veremchuk, I., Borrmann, H., Skokowski, P., Szymański, D., Grin, Y., & Kaczorowski, D. (2019). Thermal and electronic transport properties of the half-heusler phase ScNiSb. *Materials*, *12*(10). https://doi.org/10.3390/MA12101723

Tran, F., & Blaha, P. (2009). Accurate band gaps of semiconductors and insulators with a semilocal exchange-correlation potential. *Physical Review Letters*, *102*(22). https://doi.org/10.1103/PhysRevLett.102.226401

Tyuterev, V. G., & Vast, N. (2006). Murnaghan's equation of state for the electronic ground state energy. *Computational Materials Science*, *38*(2). https://doi.org/10.1016/j.commatsci.2005.08.012

Winiarski, M. J., & Bilińska, K. (2019). High thermoelectric power factors of p-type half-Heusler alloys YNiSb, LuNiSb, YPdSb, and LuPdSb. *Intermetallics*, *108*. https://doi.org/10.1016/j.intermet.2019.02.009

Xu, M., Wang, S., Yin, G., Li, J., Zheng, Y., Chen, L., & Jia, Y. (2006). Optical properties of cubic Ti3N4, Zr3N4, and Hf3N4. *Applied Physics Letters*, *89*(15). https://doi.org/10.1063/1.2360937

Yadav, M. K., & Sanyal, B. (2015). First principles study of thermoelectric properties of Li-based half-Heusler alloys. *Journal of Alloys and Compounds*, *622*. https://doi.org/10.1016/j.jallcom.2014.10.025

Yakoubi, A., Baraka, O., & Bouhafs, B. (2012). Structural and electronic

properties of the Laves phase based on rare earth type BaM 2 (M=Rh, Pd, Pt). *Results in Physics*, *2*, 58–65. https://doi.org/10.1016/j.rinp.2012.06.001

Yang, J., Li, H., Wu, T., Zhang, W., Chen, L., & Yang, J. (2008). Evaluation of half-Heusler compounds as thermoelectric materials based on the calculated electrical transport properties. *Advanced Functional Materials*, *18*(19). https://doi.org/10.1002/adfm.200701369

Yaqoob, N., Sabir, B., Murtaza, G., Arif Khalil, R. M., Muhammad, N., & Laref, A. (2019). Structural, electronic, magnetic, optical and thermoelectric response of half-metallic AMnTe2 (A = Li, Na, K): An ab-initio calculations. *Physica B: Condensed Matter*, *574*. https://doi.org/10.1016/j.physb.2019.08.033

Yu, C., Zhu, T. J., Shi, R. Z., Zhang, Y., Zhao, X. B., & He, J. (2009). High-performance half-Heusler thermoelectric materials Hf1-x ZrxNiSn1-ySby prepared by levitation melting and spark plasma sintering. *Acta Materialia*, *57*(9). https://doi.org/10.1016/j.actamat.2009.02.026

Zhang, Q., Cao, F., Liu, W., Lukas, K., Yu, B., Chen, S., Opeil, C., Broido, D., Chen, G., & Ren, Z. (2012). Heavy doping and band engineering by potassium to improve the thermoelectric figure of merit in p-type PbTe, PbSe, and PbTe 1-ySe y. *Journal of the American Chemical Society*, *134*(24), 10031–10038. https://doi.org/10.1021/ja301245b

Zhu, T., Fu, C., Xie, H., Liu, Y., & Zhao, X. (2015). High Efficiency Half-Heusler Thermoelectric Materials for Energy Harvesting. In *Advanced Energy Materials* (Vol. 5, Issue 19). https://doi.org/10.1002/aenm.201500588